JAST (Journal of Animal Science and Technology) TITLE PAGE

ARTICLE INFORMATION	Fill in information in each box below
Article Type	Research article
Article Title (within 20 words without abbreviations)	*Aporocactus flagelliformis* water extract and limonin suppresses P2Y purinoceptor 14-mediated proinflammatory features in 3D4/31 porcine alveolar macrophages
Running Title (within 10 words)	AFWE and limonin suppresses $P2Y_{14}$-mediated inflammation in porcine alveolar macrophages
Author	Hyungkuen Kim[1], Hyun Sik Jun[2], Ki-Duk Song[3], Sung-Jo Kim[1]
Affiliation	1 Department of Biotechnology, College of Life and Health Sciences, Hoseo University, Asan, Korea 2 Department of Biotechnology and Bioinformatics, College of Science and Technology, Korea University, Sejong, Republic of Korea 3 Department of Agricultural Convergence Technology, Jeonbuk National University, Jeonju 54896, Korea
ORCID (for more information, please visit https://orcid.org)	Hyungkuen Kim (https://orcid.org/0000-0001-7508-9933) Hyun Sik Jun (https://orcid.org/0000-0002-1570-7784) Ki-Duk Song (https://orcid.org/0000-0003-2827-0873) Sung-Jo Kim (https://orcid.org/0000-0003-4590-3644)
Email address	Hyungkuen Kim (20205284@vision.hoseo.edu) Hyun Sik Jun (toddjun@korea.ac.kr) Ki-Duk Song (kiduk.song@jbnu.ac.kr) Sung-Jo Kim (sungjo@hoseo.edu)
Competing interests	No potential conflict of interest relevant to this article was reported.
Funding sources State funding sources (grants, funding sources, equipment, and supplies). Include name and number of grant if available.	This work was supported by the Basic Science Research Program through the National Research Foundation of Korea (NRF) funded by the Ministry of Education(2021R1F1A1049562); and the ´R&D Program for Forest Science Technology (2021374C10-2123-BD02)´ provided by the Korea Forest Service (Korea Forestry Promotion Institute); and research funds of Jeonbuk National University in 2023.
Acknowledgements	Not applicable.
Availability of data and material	Upon reasonable request, the datasets of this study can be available from the corresponding author.
Authors' contributions Please specify the authors' role using this form.	Conceptualization: Kim H, Jun HS, Song KD, Kim SJ. Methodology: Kim H. Investigation: Kim H. Writing - original draft: Kim H. Writing - review & editing: Jun HS, Song KD, Kim SJ.
Ethics approval and consent to participate	This article does not require IRB/IACUC approval because there are no human and animal participants.

5 **CORRESPONDING AUTHOR CONTACT INFORMATION**

For the corresponding author (responsible for correspondence, proofreading, and reprints)	Fill in information in each box below
First name, middle initial, last name	Ki-Duk Song
Email address – this is where your proofs will be sent	kiduk.song@jbnu.ac.kr
Secondary Email address	kiduk.song@gmail.com
Address	567 Baek-jedaero, Deokjin gu, Jeonju, Korea
Cell phone number	+82-10-5622-1158
Office phone number	+82-63-219-5523
Fax number	+82-63-270-4739

6
7

For the corresponding author (responsible for correspondence, proofreading, and reprints)	Fill in information in each box below
First name, middle initial, last name	Sung-Jo, Kim
Email address – this is where your proofs will be sent	sungjo@hoseo.edu
Secondary Email address	sungjo@gmail.com
Address	Hoseo University, Baebang, Asan 31499, Korea
Cell phone number	+82-10-7268-9981
Office phone number	+82-41-540-5571
Fax number	+82-41-540-5898

8
9

Abstract

Respiratory diseases have been recognized as a significant cause of reduced livestock productivity since 1995. Respiratory diseases in the swine industry caused by both biological and non-biological factors are collectively referred to as porcine respiratory disease complex (PRDC). However, there is a lack of eco-friendly anti-inflammatory drugs (AIDs) that can effectively control lung inflammation caused by PRDC. P2Y purinoreceptor 14 ($P2Y_{14}$) has been identified as a key regulator of macrophage inflammatory responses; however, its regulatory role in porcine lung inflammation remains unclear. In this study, we investigated the role of $P2Y_{14}$ in inflammation in 3D4/31 PAMs and attempted to develop a novel AID. An extract of the Mexican medicinal plant *Aporocactus flagelliformis* (AFWE) reduced ROS production and pro-inflammatory cytokine expression in phorbol myristate acetate-stimulated 3D4/31-PAMs. It also reduced glucose uptake, glycogen accumulation, and expression of genes related to the $P2Y_{14}$ cascade. Polarity-based fractionation and liquid chromatography-mass spectrometry identified limonin as an anti-inflammatory compound in AFWE. Limonin reduced P2RY14 and proinflammatory gene expression induced by the $P2Y_{14}$ ligand UDPG in 3D4/31-PAMs, demonstrating its inhibitory effect on $P2Y_{14}$-mediated inflammation. These results suggest that $P2Y_{14}$ is an inflammatory receptor in PAMs and an effective target for AID development. We also propose AFWE and limonin as candidate AIDs for pigs.

Keywords: Porcine respiratory disease complex, Porcine alveolar macrophages, inflammation, $P2Y_{14}$, Aporocactus flagelliformis, limonin

INTRODUCTION

The porcine respiratory disease complex (PRDC) causes economic losses in the swine industry by reducing pork production efficiency and increasing feed costs, carcass disposal costs, and medical expenses [1]. Various factors, including overcrowded rearing conditions, porcine circovirus type 2 (PCV2), porcine reproductive and respiratory syndrome virus, swine influenza virus, *Mycoplasma hyopneumoniae*, and *Pasteurella multocida* influence the onset of PRDC [2]. Infections by PRDC-related viruses lead to proinflammatory cytokine expression and tissue damage in porcine lungs [3], which can be alleviated by anti-inflammatory drugs (AIDs). However, the development and selection of suitable AIDs for PRDC are limited because of a lack of research [4]. Therefore, in this study, we aimed to develop an AID for porcine.

Inflammation caused by infection is primarily mediated by macrophages. PCV2 targets macrophage populations, including alveolar macrophages (AMs), and induces a strong inflammatory response [5]. Increased expression of NOX2, which mediates reactive oxygen species (ROS) production, has been reported in PCV2-infected macrophages [6]. This induces autophagy and PCV2 replication, which can be inhibited by blocking autophagy or ROS [7, 8]. Additionally, PCV2-infected macrophages show increased expression of proinflammatory cytokines, including tumor necrosis factor-α (TNFα) and cyclooxygenase-2 (COX2) [9]. The acute inflammatory response in macrophages is mediated by P2Y purinoceptor 14 ($P2Y_{14}$), which is a member of the pyrimidinergic G protein-coupled receptor family. Activation of $P2Y_{14}$ by uridine-5′-diphosphoglucose (UDPG), which is produced and secreted during glycogenesis, induces the expression of signal transducer and activator of transcription 1 (STAT1) and TNFα [10]. Although the ability of $P2Y_{14}$ to recognize UDPG has been reported in porcine coronary arteries [11], the role of $P2Y_{14}$ in porcine macrophages (PAMs) is unclear.

With the global ban on antibiotics in animal feed, there has been increased attention on developing eco-friendly antibacterial and anti-inflammatory strategies to maintain porcine health and productivity [12]. Succulent plants, which are also used as porcine feed, have shown some anti-inflammatory effects in porcine cells and are emerging as natural anti-inflammatory agents [13-15]. The succulent *Aporocactus flagelliformis* (*A. flagelliformis*), also known as rattail cactus, is traditionally used in Mexico to treat heart disease and diabetes [16, 17]. Inhibition of $P2Y_{14}$ in porcine shows potential for treating these conditions [11, 18]. Here, we focused on the therapeutic effects of *A. flagelliformis* on $P2Y_{14}$ and various diseases.

In this study, we developed *an A. flagelliformis* water extract (AFWE) and investigated its anti-inflammatory effects on 3D4/31-PAMs, including ROS production, proinflammatory cytokine expression, and bactericidal activity.

We also evaluated the effects of AFWE on $P2Y_{14}$ metabolism. Limonin was identified using liquid chromatography-mass spectrometry (LC-MS) as a major compound of AFWE. The binding potential of limonin to porcine $P2Y_{14}$ was assessed and the therapeutic effects of limonin on UDPG-induced inflammation were evaluated.

MATERIALS AND METHODS

Preparation of *A. flagelliformis* water extract

Fresh *A. flagelliformis* (Xplant, Seoul, Korea) was cut into 2-3 cm lengths, washed with deionized water (dH_2O), and extracted with dH_2O (300 mL dH_2O for 100 g *A. flagelliformis*) for 15 min at 110 °C using a WAC-60 autoclave (Daihan Scientific, Wonju-si, Gangwon-do, Korea). The aqueous phase was collected, sterile filtered using a 0.2 μm cellulose-acetate filter (16534-K, Minisart, Sartorius, Goettingen, Germany), and stored at -80 °C before use.

Cell culture condition

3D4/31 porcine alveolar macrophages (3D4/31-PAMs; ATCC-CRL-2844; ATCC, Manassas, VA, USA) and A549 human alveolar epithelial cells (A549-AECs; CCL-185, ATCC) were maintained in a 5 % CO_2 atmosphere at 36.5 °C. Cells were grown in a 4:6 ratio of Dulbecco's modified Eagle's medium (10-013-CVR, Corning, Corning, NY, USA) and Roswell Park Memorial Institute (RPMI) 1640 medium (10-040-CVR, Corning) supplemented with 10 % (v/v) fetal bovine serum (TMS-013, Merck Millipore, Burlington, MA, USA) and 1 % (v/v) penicillin-streptomycin (LS202-02, Welgene, Gyeongsan-si, Gyeongsangbuk-do, Korea).

Drugs and treatment

Cells were cultured for 12 h prior to treatment. Cells were treated for 24 h, refreshed medium/treatment, and stimulated with 2 nM phorbol myristate acetate (PMA; P1585-1MG, Sigma-Aldrich, St. Louis, MO, USA). The treatments included 60 μg/mL AFWE, 30 μM limonin (A10531, Adooq Bioscience, Irvine, CA, USA), and 200 μM UDPG (U4625-25MG, Sigma-Aldrich). Limonin was prepared at a final concentration of 50 mM in 99.9 % dimethyl sulfoxide (DMSO; sterile, cell culture grade).

Quantification of cell viability and proliferation

To quantify cell viability, cells were cultured with 10 % (v/v) water-soluble tetrazolium salt-8 (WST8) reagent (QM2500, BIOMAX, Seoul, Korea) for 2 h, and the optical density at 450 nm (OD_{450}) was measured using a FilterMax F3 microplate reader (Molecular Devices, San Jose, CA, USA). For quantification of proliferation, cells were harvested and stained with 0.2 % (v/v) trypan blue (15250-061, Gibco, North Andover, MA, USA) for 1 min, and viable cells were counted using a hemocytometer.

Measurement of intracellular ROS level

Cells were cultured with 1 μM 2′,7′-dichlorofluorescein diacetate (H_2DCFDA; 35845, Sigma-Aldrich) for 30 min, washed with phosphate-buffered saline (PBS; pH 7.4), harvested, washed with PBS, and analyzed by flow cytometry.

Immunoblotting and densitometry analysis

Cells were lysed in radioimmunoprecipitation assay buffer containing 1 mM phenylmethanesulfonyl fluoride (P7626-5G, Sigma-Aldrich) for 1 h at 4 °C. The supernatant was collected by centrifugation at 14,000 RCF for 15 min. Protein concentration was quantified using Bradford's assay with a bovine serum albumin (BSA; 10735086001, Roche, Basel, Switzerland) standard. Proteins were separated by sodium dodecyl sulfate polyacrylamide gel electrophoresis and transferred onto polyvinylidene fluoride membranes (3010040001, Roche) using a HorizeBLOT 2M transfer system (ATTO, Tokyo, Japan). Membranes were blocked with 5 % (w/v) skim milk, washed with tris-buffered saline [TBST; pH 7.6, 0.05 % (v/v) Tween 20], and probed with primary antibodies at 4 °C for 12 h. Membranes were then washed with TBST, proved with secondary antibodies, and washed with TBST. The membranes were then exposed to an enhanced chemiluminescence reagent, visualized using an X-ray film (EA8EC, AGFA, Mortsel, Belgium), and quantified by densitometry analysis using ImageJ Ver. 1.5.3q (National Institutes of Health, Bethesda, MD, USA). The antibodies used for immunoblotting are listed in Table 1.

RNA isolation and quantitative real-time PCR (qRT-PCR)

All procedures were performed according to the manufacturer's instructions. RNA was isolated using TRIzol reagent (15596026, Invitrogen, Carlsbad, CA, USA), quantified using NanoDrop, and converted to cDNA at a concentration of 1 μg using Oligo dT20 primers with the WizScript cDNA Synthesis Kit (W2202, Wizbiosolutions, Seongnam-si, Gyeonggi-do, Korea). cDNA was quantified using SYBR Green qPCR Master Mix (DQ485; BioFACT,

Daejeon, Korea), StepOnePlus RT-PCR System (Applied Biosystems, Foster City, CA, USA), and StepOne software Ver. 2.3. The fold change in mRNA expression was normalized to *ribosomal protein S29* (*RPS29*) using the $2^{(-\Delta\Delta Ct)}$ method. The primer sequences used for qRT-PCR are listed in Table 2.

In vitro bactericidal assay

3D4/31-PAMs (1×10^6 cells), *Escherichia coli* (*E. coli*) DH5α (1×10^7 CFU, colony forming unit), and 5 % (v/v) porcine serum were mixed in a final volume of 1 mL of Hanks' balanced salt solution (HBSS, pH 7.4) and incubated at 37 °C for 1 h with shaking (180 rpm). After centrifugation at 12,000 RCF for 1 min, the supernatant (non-engulfed bacteria) was spread onto Luria-Bertani (LB; 244602, BD, Detroit, MI, USA) agar plates. The pelleted cells (with engulfed bacteria) were washed twice with HBSS, suspended in 1 mL of RPM1640 medium, and incubated for 0, 20, and 40 min at 37 °C with shaking (180 rpm). After each incubation period, the cells were lysed with dH_2O for 5 min and spread on LB agar plates. The CFUs were counted after incubation for 12 h at 37 °C. Images of the LB agar plates were captured using iPhone X (Apple, Cupertino, CA, USA).

Measurement of autophagic activity

Cells were cultured with 1 μg/mL acridine orange (A6014, Sigma-Aldrich) for 15 min, washed twice with PBS, harvested, washed with PBS, and analyzed by flow cytometry.

Glucose uptake assay

Cells were suspended in PBS containing 50 μM 2-NBD-glucose (2-NBDG; 11046-10MG, Cayman Chemical, Ann Arbor, MI, USA) and 0.1 % (w/v) BSA, incubated for 30 min, washed with PBS, and analyzed by flow cytometry.

Measurement of intracellular lipid droplet content

Cells were cultured with 1 μM $BODIPY^{493/503}$ (D3922, Invitrogen) for 30 min, washed twice with PBS, and subjected to fluorescence microscopy or flow cytometry. For flow cytometry, cells were harvested, washed with PBS, and analyzed.

Visualization and quantification glycogen

Glycogens were visualized using Best's carmine staining [19] with minor modifications. Cells were fixed for 15

min with 3.8 % (w/v) formaldehyde, washed with PBS, and stained with 0.625 % (w/v) Best's carmine solution (C1022; Sigma-Aldrich) for 30 min. Cells were then rinsed twice with dH_2O containing 2 % (v/v) methanol and 4 % (v/v) ethanol, washed with ethanol for 1 min, and imaged. Glycogen content was quantified using the anthrone method [20] with minor modifications. Cells (1×10^5) were lysed in 50 µL of 30 % (w/v) KOH for 20 min at 100 °C and 350 µL of 43 % (v/v) ethanol was added. The cell lysate (50 µL) was reacted with 100 µL of 0.2 % (w/v) anthrone (319899, Sigma-Aldrich) at 100 °C for 20 min. The OD_{620} of the lysate and glucose (G8270, Sigma-Aldrich) standards were measured using a FilterMaxF3 microplate reader.

Fractionation of AFWE

Serial fractionation of AFWE was performed using ethyl acetate, ethyl ether, ethanol, and isopropyl ether (extra-pure grade). The AFWE was shaken in a specific solvent system for 10 min and allowed to stand at 25 °C until the mixture formed two layers (1-2 h). The organic layer was then concentrated to 20 × in DMSO using a rotary evaporator.

LC-MS of AFWE

LC was carried out using an Acquity UPLC system (Waters, Milford, MA, USA) with an Acquity BEH C18 1.7 µm column (2.1 × 100 mm). The LC processed the samples at 0.2 mL/min using water/methanol with 0.1 % (v/v) formic acid at 40 °C. MS was performed using the SYNAPT G2 platform (Waters). Molecules were identified using m/z CLOUD (https://www.mzcloud.org) and molecular structures were illustrated using ChemDraw Ultra Ver. 12.0.2 (CambridgeSoft, Cambridge, MA, USA).

Computational prediction of molecular docking

The 3D structure of porcine-$P2Y_{14}$ (AF-F1SJN3-F1) was downloaded from the AlphaFold Protein Structure Database Ver. 2022-11-01 (https://alphafold.ebi.ac.uk). The canonical SMILES of the ligands (Limonin #179651 and UDPG #8629, PubChem release 2021.10.14) were retrieved from the PubChem Database (https://pubchem.ncbi.nlm.nih.gov). Molecular docking and visualization were performed using DiffDock-L [21] hosted at Neurosnap.ai (https://neurosnap.ai).

Flow cytometry analysis

Flow cytometry was performed using a Guava easyCyte Flow Cytometer (Merck Millipore) and Guava InCyte

software Ver. 2.6. An average of 3×10^3 cells was measured for the single-channel assay and an average of 5×10^3 cells was measured for the dual-channel assay. Flow cytometry plots and fluorescence intensities were obtained using the FlowJo Ver. 10.6.2 (TreeStar, Ashland, OR, USA).

Imaging and processing

Microscopy was performed using DMi8 fluorescence microscope (Leica, Wetzlar, Germany). LAS X software Ver. 2.0.0.14332 was used for the fluorescence images, and LAS software Ver. 4.7.1 for the bright-field images. To display representative images, contrast and brightness adjustments were processed using Photoshop 2024 (Adobe Systems, San Jose, CA, USA).

Statistical analysis

Statistical analyses were based on at least 3 independent biological experiments and were performed using GraphPad PRISM software Ver. 10.2.3 (GraphPad Software, San Diego, CA, USA). All data are shown as mean ± standard deviation. Analysis of variance (ANOVA) with Tukey's multiple comparison test or unpaired two-tailed Student's t-test was used for statistical analyses. Statistical significance was set at $p < 0.05$.

RESULTS

***A. flagelliformis* water extract suppresses proinflammatory features in 3D4/31-PAMs**

To determine the anti-inflammatory properties of *A. flagelliformis*, we developed AFWE and evaluated its bioactivity against ROS production, cytokine expression, and bactericidal activity in 3D4/31-PAMs. First, fresh *A. flagelliformis* was extracted using a water extraction method (Fig. 1A and 1B). The dry weight of AFWE was found to be 6 mg/mL, giving an extraction efficiency of 1.8% based on the solid content. To determine the cytotoxicity of AFWE on pulmonary alveoli, WST8 was performed on 3D4/31-PAM and A549-AEC. Although AFWE was not cytotoxic to 3D4/31-PAMs, A549-AECs viability was increased by 60 μg/mL AFWE and decreased by 6 μg/mL AFWE treatment (Fig. 1C). As the number of tissue-resident AMs decreases with the severity of lung infection [22, 23], we tested the protective effect of AFWE on the proliferation of 3D4/31-PAMs. However, 60 μg/mL AFWE did not upregulate the proliferation of PMA-stimulated 3D4/31-PAMs (PS-3D4/31-PAMs) (Fig. 1D).

AFWE (0.006-60 μg/mL) reduced the intracellular ROS levels in PS-3D4/31-PAMs (Fig. 1E). 60 μg/mL AFWE showed no antioxidant effect on unstimulated 3D4/31-PAMs (Fig. 1F). This antioxidant effect of AFWE on PS-3D4/31-PAM is supported by the inhibition of NADPH oxidase 2 (NOX2) complex expression, a source of ROS, in inflamed AMs [24]. AFWE (60 μg/mL) suppressed the expression of NOX2 complex, including $gp91^{PHOX}$ (NOX2) (Fig. 1G), *neutrophil cytosolic factor 2* (*NCF2)*, *NCF1*, *NCF4*, and *cytochrome b-245 α chain* (*CYBA*) in PS-3D4/31-PAMs (Fig. 1H). Overall, 60 μg/mL AFWE lowered ROS production via the downregulation of NOX2 without toxicity in 3D4/31-PAM. Furthermore, AFWE treatment at concentrations lower than 60 μg/mL was toxic in A549-AEC, so we established 60 μg/mL as the optimal AFWE concentration for alveolar immunomodulation and conducted subsequent experiments.

Next, we confirmed that AFWE inhibited proinflammatory gene expression and bactericidal activity in 3D4/31-PAMs. AFWE decreased the levels of proinflammatory markers such as COX2 (Fig. 2A), *prostaglandin-endoperoxide synthase 2* (*PTGS2*), *TNF*, and *interleukin 1 β* (*IL1B*) (Fig. 2B) in PS-3D4/31-PAMs while slightly reducing the expression of the anti-inflammatory marker *ARG1* and *resistin-like β* (*RETNLB*) (Fig. 2B). Bactericidal assays (Fig. 2C) revealed that AFWE diminished the bactericidal activity against *E. coli* DH5α in 3D4/31-PAMs (Fig. 2D and 2E). Moreover, AFWE reduced *the E. coli*-induced autophagy (Fig. 2F). These results indicate that AFWE downregulates proinflammatory features, including ROS production, proinflammatory gene expression, and bactericidal activity, in 3D4/31-PAMs.

A. flagelliformis water extract suppresses $P2Y_{14}$-associated metabolism in 3D4/31-PAMs

To confirm whether AFWE regulates $P2Y_{14}$-associated metabolism in PAMs, glucose metabolism and $P2Y_{14}$ cascade were quantified. Glucose uptake was reduced (Fig. 3A), and the LD content was upregulated (Fig. 3B and 3C) by AFWE in the 3D4/31-PAMs. The increased glycogen content in 3D4/31-PAMs following PMA stimulation was prevented by AFWE treatment (Fig. 3D and 3E). Considering that lipid accumulation in polarized macrophages depends on fatty acid uptake [25], our results indicate that AFWE selectively blocks $P2Y_{14}$ (glycogen)-mediated inflammation. Glucose uptake, glycogenesis, and the pentose phosphate pathway (PPP) are essential for $P2Y_{14}$-mediated proinflammatory responses. In particular, activation of the glycogenesis, characterized by intracellular glycogen accumulation, is required for the production of the $P2Y_{14}$ ligand UDPG [10] (Fig. 3F). qRT-PCR showed that AFWE suppressed the expression of genes related to glucose uptake (*SLC2A1*, *solute carrier family 2 member 1*), glycogenesis (*PGM1*, *phosphoglucomutase 1*; *PYGL*, *glycogen phosphorylase L*; *GAA*, *α-glucosidase*), and PPP

(*G6PD*, *glucose-6-phosphate dehydrogenase*; *TKT*, *transketolase*) in the 3D4/31-PAMs (Fig. 3G and 3H). AFWE suppressed *P2RY14* and *STAT1* expression in the PS-3D4/31-PAMs (Fig. 3I), suggesting that AFWE suppresses metabolism related to $P2Y_{14}$ activation. These results suggest that AFWE suppresses $P2Y_{14}$-associated proinflammatory features in PAMs

Identification of potential $P2Y_{14}$ antagonistic compound in *A. flagelliformis* water extract

Polarity-based fractionation and LC-MS were performed to identify anti-inflammatory compounds in AFWE. The obtained fractions were concentrated 20-fold before use, and the dry weight of AFWE-OL3 was 52 mg/mL (Fig. 4A). AFWE-OL3 (52 μg/mL) reduced the levels of $P2Y_{14}$ and PYGL in the immunoblotting of 3D4/31-PAMs (Fig. 4B). Genetic or chemical inhibition of PYGL can effectively inhibit $P2Y_{14}$-mediated cytokine expression by reducing NADPH production [10]. The LC chromatogram of AFWE-OL3 showed a major peak at retention time (RT) 9.56 (Fig. 4C). The mass spectrum of RT9.56 was analyzed using the m/z CLOUD Mass Spectral Database, and the most similar compound was identified as limonin, also known as obaculactone and evodin (Fig. 4D). Based on the peak area (39%) at RT 9.56, AFWE-OL3 is expected to contain 28.42 mg/mL limonin. Considering that AFWE-OL3 was 20-fold enriched, it is estimated that limonin is present in AFWE at a concentration of 1.42 mg/mL. Limonin (Fig. 4E), a limonoid polyphenol found in citrus, has been reported to protect against lipopolysaccharide (LPS)-induced acute lung injury [26]. Interestingly, in citrus fruits, the glucose unit of UDPG can be transferred to limonin by limonoid glucosyltransferase [27].

To assess the potential interaction between limonin and porcine-$P2Y_{14}$, we performed computational molecular docking analysis. The structure of the porcine-$P2Y_{14}$ (Fig. 4F) used in this study exhibited a very high confidence for ARG253/LYS277/GLU278 (Fig. 4G), a key amino acid in the interaction between $P2Y_{14}$ and UDPG [28]. Our prediction showed that UDPG interacts with ARG253/LYS277/GLU278 in porcine-$P2Y_{14}$ (Fig. 4H). The prediction of limonin docking to porcine-$P2Y_{14}$ showed consistency in limonin poses (Fig. 4I). The prediction model with the highest score showed an interaction between limonin and ARG253/LYS277 (Fig. 4J). These results suggest the potential binding of limonin to the UDPG-binding site of porcine-$P2Y_{14}$.

Limonin suppresses UDPG-induced proinflammatory gene expression in 3D4/31-PAMs

To confirm the anti-inflammatory effect of limonin on PAMs, we assessed the dose-response effect of limonin on viability and proinflammatory gene expression. Limonin treatment, at a final concentration of 30 μM, increased

the viability of 3D4/31-PAMs cultured with or without PMA (Fig. 5A). Dose-response screening of limonin using qRT-PCR showed that 30 μM limonin suppressed the expression of *P2RY14*, *STAT1*, *and PTGS2*, but not *ARG1*, in PS-3D4/31-PAMs (Fig. 5B). Based on these results, we suggest that limonin at a final concentration of 30 μM has the potential to suppress $P2Y_{14}$-mediated inflammation in PAMs.

Next, to assesses the effects of limonin on UDPG-induced inflammation, 3D4/31-PAMs were stimulated with combination of PMA with UDPG. Significantly increased expression levels of *retinoic acid receptor β* (RARB), *STAT1*, *PTGS2*, and arginase-1 (*ARG1*) were observed in 3D4/31-PAMs stimulated with 200 μM UDPG. Limonin treatment suppressed the expression of *P2RY14*, *RARB*, *STAT1*, *PTGS2*, and *ARG1* in 3D4/31-PAMs stimulated with PMA/UDPG (200 μM) (Fig. 5C). The PMA/UDPG-induced ROS production in 3D4/31-PAMs was reduced by limonin treatment (Fig. 5D). These results suggest that limonin has the potential to suppress UDPG/$P2Y_{14}$-induced inflammation in PAMs.

DISCUSSION

PRDC remain the most serious threat to pig health and productivity. This study sought to explore the association of $P2Y_{14}$ with porcine respiratory inflammation and to develop a new AID. AFWE inhibited ROS production by reducing the expression of NOX family members in PS-3D4/31-PAMs and suppressed glucose uptake and glycogenesis. We also demonstrated the potential of AFWE to inhibit $P2Y_{14}$-mediated inflammation by reducing the expression of *P2RY14*, *STAT1*, *TNF*, *ILB1*, and *PTGS2*. Limonin reduced the UDPG-induced expression of *P2RY14*, *RARB*, *STAT1*, and *PTGS2* in 3D4/31-PAMs. These results suggest the involvement of $P2Y_{14}$ as a major regulator of inflammatory responses in PAMs and propose AFWE and limonin as AID candidates that can control this receptor.

Macrophages under inflammatory stimuli or after phagocytosis of bacteria increase cytokine and ROS production to recruit immune cells and eliminate pathogens [29]. AFWE inhibited NOX2 complex expression, ROS production, and bactericidal activity in 3D4/31-PAMs. These results are consistent with reports that NOX2 is a major source of ROS that kills phagocytic bacteria and that NOX2 deficiency impairs bactericidal activity [30]. AFWE inhibited the expression of proinflammatory genes *PTGS2*, *TNF*, and *IL1B* in 3D4/31-PAMs. TNF and IL1B induce macrophage activation and *PTGS2* expression. COX2 (encoded by *PTGS2*) is a major target for anti-inflammatory drug development, as it plays a central role in the regulation of inflammatory processes through the modulation of vascular permeability and tissue swelling [31]. Therefore, the inhibitory effect of AFWE and limonin on PTGS2 expression

suggests their potential as anti-inflammatory drugs. ARG1 expression was increased by PMA in 3D4/31-PAMs and slightly reduced by AFWE. ARG1 is classically used as a marker of anti-inflammation; however, AMs have been reported to express both inflammatory and anti-inflammatory markers and express high levels of ARG1 under chronic infection [32, 33]. Therefore, we suggest that the increase in *ARG1* levels by PMA and UDPG is due to the metabolic features of AMs.

Glucose is essential for energy metabolism and $P2Y_{14}$-mediated inflammation. AFWE slightly decreased the glucose uptake of 3D4/31-PAMs but increased the LD content and had no effect on viability and proliferation. Given the high dependence of AMs proliferation and development on fatty acid metabolism [34], we suggest that activation of fatty acid metabolism may have maintained energy metabolism. PMA treatment increased *SLC2A1* expression but decreased glucose uptake and did not increase $P2Y_{14}$ cascade gene expression. PMA/UDPG treatment increased *RARB* and *STAT1* expression, suggesting that $P2Y_{14}$-mediated inflammation was activated. These results suggest that PMA is inadequate to induce $P2Y_{14}$ activation at the mRNA expression level, and that PMA/UDPG combination treatment is suitable for $P2Y_{14}$ activation in 3D4/31-PAM.

Increased $P2Y_{14}$ activity is closely related to the exacerbation of various diseases including asthma [35], coronavirus disease 2019 [36], gouty arthritis [37], and intestinal inflammation [38], suggesting a variety of therapeutic uses for $P2Y_{14}$ antagonists. In porcine, $P2Y_{14}$ has been reported as a therapeutic target for heart disease and diabetes [11, 18], and we demonstrated its role in porcine alveolar immunity. We observed increased glycogenesis, a characteristic feature of $P2Y_{14}$-mediated inflammation, in PS-3D4/31-PAMs. These results suggest an increased glucose requirement by macrophages in inflammatory responses, and are consistent with LPS-induced increased glucose consumption and hypoglycemia [39]. Additionally, porcine skeletal muscle growth rate is associated with the expression of glycogenesis-related genes (*PGM1*, *phosphoglucomutase 1*; *UGP2*, *UDPG pyrophosphorylase 2*) [40]. These findings make it interesting to study the effects of $P2Y_{14}$ and UDPG levels on porcine productivity.

The selection of extraction solvents considers various factors such as extraction efficiency, environmental hazards, and residual toxicity. In line with the global trend toward eco-friendly industries, the importance of water extraction technology is increasing [41]. Succulent *Opuntia* species, known to have potential as livestock feed [13], have been reported to lack antioxidant and antibacterial effects in aqueous extracts [42]. This is attributed to the low solubility of major bioactive compounds such as polyphenols in water [43]. Using LC-MS, we identified limonin as a potential bioactive compound in AFWE. Limonin can be extracted from *Citrus grandis* (pomelo) via water and resin absorption [44]. Additionally, limonin is abundant in the peel of *Citrus aurantifolia* (lime), which is often discarded as waste and

317 can be extracted using the low-toxicity solvent, ethanol [45]. In this study, the limonin content of AFWE estimated by
318 LC-MS was 23.69% (w/v), 1.42 mg/mL. A 14.21 μg/mL of limonin content was expected with 60 μg/mL AFWE
319 treatment, which was similar to the optimal anti-inflammatory activity concentration of 30 μM (14.12 μg/mL) of
320 limonin. This suggests that limonin confers anti-inflammatory activity to AFWE. Overall, these findings suggest that
321 AFWE and limonin are promising AID candidates for the eco-friendly livestock industry.

322 Limonin has been noted for its various pharmacological activities but has limited clinical potential due to unclear
323 mechanisms of action [46]. In this study, we confirmed that AFWE and limonin reduced PMA-induced expression of
324 *PTGS2*, *STAT1*, and *P2RY14* in 3D4/31-PAMs. Our molecular docking prediction also indicated that limonin has a
325 higher binding score to porcine-$P2Y_{14}$ than to UDPG. These results suggest that the potential mechanism of action
326 (MOA) of AFWE and limonin involves binding to and inhibiting the activity of porcine-$P2Y_{14}$. Further research is
327 required to clarify this MOA, including confirmation of the nuclear localization of STAT1/RARβ, which is
328 characteristic of $P2Y_{14}$ activation [10]. Our molecular docking analysis used the predicted porcine-$P2Y_{14}$ structure
329 due to the limited number of studies on porcine-$P2Y_{14}$. Although UDPG binding to $P2Y_{14}$ induces structural changes
330 [28], mechanical binding studies of limonin to porcine-$P2Y_{14}$ have not been conducted. Nevertheless, the reduction in
331 the UDPG-induced expression of *RARB*, *STAT1*, and *PTGS2* in 3D4/31-PAMs by limonin suggests the potential of
332 limonin to inhibit $P2Y_{14}$-mediated inflammation.

333 In summary, AFWE exerted anti-inflammatory effects in 3D4/31-PAMs, inhibiting ROS production and
334 *NOX2*/*PTGS2*/*TNFA* expression reported in PRDC. Limonin, a compound identified from AFWE, inhibited the
335 UDPG-induced expression of $P2Y_{14}$ cascade genes and *PTGS2* in 3D4/31-PAMs. Overall, our results suggest that
336 $P2Y_{14}$ is a target for the control of PRDC and provides new insights into the inflammatory response of PAMs.
337 Furthermore, we propose AFWE and limonin as candidate AIDs for porcine.

338

339

340

REFERENCES

1. Calderon Diaz JA, Fitzgerald RM, Shalloo L, Rodrigues da Costa M, Niemi J, Leonard FC, et al. Financial Analysis of Herd Status and Vaccination Practices for Porcine Reproductive and Respiratory Syndrome Virus, Swine Influenza Virus, and Mycoplasma hyopneumoniae in Farrow-to-Finish Pig Farms Using a Bio-Economic Simulation Model. Front Vet Sci. 2020;7:556674. https://doi.org/10.3389/fvets.2020.556674.

2. Hansen MS, Pors SE, Jensen HE, Bille-Hansen V, Bisgaard M, Flachs EM, Nielsen OL. An investigation of the pathology and pathogens associated with porcine respiratory disease complex in Denmark. J Comp Pathol. 2010;143(2-3):120-31. https://doi.org/10.1016/j.jcpa.2010.01.012.

3. Sanchez-Carvajal JM, Rodriguez-Gomez IM, Ruedas-Torres I, Larenas-Munoz F, Diaz I, Revilla C, et al. Activation of pro- and anti-inflammatory responses in lung tissue injury during the acute phase of PRRSV-1 infection with the virulent strain Lena. Vet Microbiol. 2020;246:108744. https://doi.org/10.1016/j.vetmic.2020.108744.

4. Schoos A, Devreese M, Maes DG. Use of non-steroidal anti-inflammatory drugs in porcine health management. Vet Rec. 2019;185(6):172. https://doi.org/10.1136/vr.105170.

5. Chang HW, Jeng CR, Lin TL, Liu JJ, Chiou MT, Tsai YC, et al. Immunopathological effects of porcine circovirus type 2 (PCV2) on swine alveolar macrophages by in vitro inoculation. Vet Immunol Immunopathol. 2006;110(3-4):207-19. https://doi.org/10.1016/j.vetimm.2005.09.016.

6. Su ZJ, Yang J, Luo WJ, Wei YY, Shuai XH, Hu TJ. Inhibitory effect of Sophora subprosrate polysaccharide on mitochondria oxidative stress induced by PCV-2 infection in RAW264.7 cells. Int J Biol Macromol. 2017;95:608-17. https://doi.org/10.1016/j.ijbiomac.2016.11.101.

7. Zhai N, Liu K, Li H, Liu Z, Wang H, Korolchuk VI, et al. PCV2 replication promoted by oxidative stress is dependent on the regulation of autophagy on apoptosis. Vet Res. 2019;50(1):19. https://doi.org/10.1186/s13567-019-0637-z.

8. Liu D, Lin J, Su J, Chen X, Jiang P, Huang K. Glutamine Deficiency Promotes PCV2 Infection through Induction of Autophagy via Activation of ROS-Mediated JAK2/STAT3 Signaling Pathway. J Agric Food Chem. 2018;66(44):11757-66. https://doi.org/10.1021/acs.jafc.8b04704.

9. Yang J, Cao MX, Hu WY, Wei YY, Hu TJ. Sophora subprosrate polysaccharide suppress the inflammatory reaction of RAW264.7 cells infected with PCV2 via regulation NF-κB/MAPKs/c-Jun signal pathway and histone acetylation modification. Int J Biol Macromol. 2020;159:957-65. https://doi.org/10.1016/j.ijbiomac.2020.05.128.

10. Ma J, Wei K, Liu J, Tang K, Zhang H, Zhu L, et al. Glycogen metabolism regulates macrophage-mediated acute inflammatory responses. Nat Commun. 2020;11(1):1769. https://doi.org/10.1038/s41467-020-15636-8.

11. Abbas ZSB, Latif ML, Dovlatova N, Fox SC, Heptinstall S, Dunn WR, Ralevic V. UDP-sugars activate P2Y(14) receptors to mediate vasoconstriction of the porcine coronary artery. Vascul Pharmacol. 2018;103-105:36-46. https://doi.org/10.1016/j.vph.2017.12.063.

12. Wang J, Lyu W, Zhang W, Chen Y, Luo F, Wang Y, et al. Discovery of natural products capable of inducing porcine host defense peptide gene expression using cell-based high throughput screening. J Anim Sci Biotechnol. 2021;12(1):14. https://doi.org/10.1186/s40104-020-00536-0.

13. Pastorelli G, Serra V, Vannuccini C, Attard E. Opuntia spp. as Alternative Fodder for Sustainable Livestock Production. Animals (Basel). 2022;12(13). https://doi.org/10.3390/ani12131597.

14. Xu Z, Liu Y, Peng P, Liu Y, Huang M, Ma Y, et al. Aloe extract inhibits porcine epidemic diarrhea virus in vitro and in vivo. Vet Microbiol. 2020;249:108849. https://doi.org/10.1016/j.vetmic.2020.108849.

15. Kim H, Jeon EH, Park BC, Kim SJ. Dudleya brittonii extract promotes survival rate and M2-like metabolic change in porcine 3D4/31 alveolar macrophages. Asian-Australas J Anim Sci. 2019;32(11):1789-800. https://doi.org/10.5713/ajas.19.0251.

16. Lozoya X. Mexican medicinal plants used for treatment of cardiovascular diseases. Am J Chin Med. 1980;8(01n02):86-95. https://doi.org/10.1142/s0192415x80000074.

17. Andrade-Cetto A, Heinrich M. Mexican plants with hypoglycaemic effect used in the treatment of diabetes. J Ethnopharmacol. 2005;99(3):325-48. https://doi.org/10.1016/j.jep.2005.04.019.

18. Alsaqati M, Latif ML, Chan SL, Ralevic V. Novel vasocontractile role of the P2Y(1)(4) receptor: characterization of its signalling in porcine isolated pancreatic arteries. Br J Pharmacol. 2014;171(3):701-13. https://doi.org/10.1111/bph.12473.

19. Horobin R, Murgatroyd L. The staining of glycogen with Best's Carmine and similar hydrogen bonding dyes. A mechanistic study. Histochem J. 1971;3:1-9. https://doi.org/10.1007/BF01686501.

20. Carroll NV, Longley RW, Roe JH. The determination of glycogen in liver and muscle by use of anthrone reagent. J biol Chem. 1956;220(2):583-93. https://doi.org/10.1016/S0021-9258(18)65284-6.

21. Corso G, Stärk H, Jing B, Barzilay R, Jaakkola T. Diffdock: Diffusion steps, twists, and turns for molecular docking. arXiv. 2022. https://doi.org/10.48550/arXiv.2210.01776.

22. Chen ST, Park MD, Del Valle DM, Buckup M, Tabachnikova A, Thompson RC, et al. A shift in lung macrophage composition is associated with COVID-19 severity and recovery. Science Translational Medicine. 2022;14(662). https://doi.org/ARTN eabn5168

10.1126/scitranslmed.abn5168.

23. de Oliveira VLS, Pollenus E, Berghmans N, Queiroz CM, Blanter M, Mattos MS, et al. Absence of CCR2 Promotes Proliferation of Alveolar Macrophages That Control Lung Inflammation in Acute Respiratory Distress Syndrome in Mice. Int J Mol Sci. 2022;23(21). https://doi.org/ARTN 1292010.3390/ijms232112920.

24. Caceres L, Paz ML, Garces M, Calabro V, Magnani ND, Martinefski M, et al. NADPH oxidase and mitochondria are relevant sources of superoxide anion in the oxinflammatory response of macrophages exposed to airborne particulate matter. Ecotoxicol Environ Saf. 2020;205:111186. https://doi.org/10.1016/j.ecoenv.2020.111186.

25. Knight M, Braverman J, Asfaha K, Gronert K, Stanley S. Lipid droplet formation in Mycobacterium tuberculosis infected macrophages requires IFN-gamma/HIF-1alpha signaling and supports host defense. PLoS Pathog. 2018;14(1):e1006874. https://doi.org/10.1371/journal.ppat.1006874.

26. Liang H, Liu G, Fan Q, Nie Z, Xie S, Zhang R. Limonin, a novel AMPK activator, protects against LPS-induced acute lung injury. Int Immunopharmacol. 2023;122:110678. https://doi.org/10.1016/j.intimp.2023.110678.

27. Karim MR, Hashinaga F. Isolation and characterization of limonoid glucosyltransferase from pummelo albedo tissue. Food Chem. 2002;76(4):431-6. https://doi.org/10.1016/S0308-8146(01)00300-4.

28. Zhao L, Wei F, He X, Dai A, Yang D, Jiang H, et al. Identification of a carbohydrate recognition motif of purinergic receptors. Elife. 2023;12. https://doi.org/10.7554/eLife.85449.

29. Nonnenmacher Y, Hiller K. Biochemistry of proinflammatory macrophage activation. Cell Mol Life Sci. 2018;75(12):2093-109. https://doi.org/10.1007/s00018-018-2784-1.

30. Márquez JDR, Li TYN, McCluggage ARR, Tan JMJ, Muise A, Higgins DE, Brumell JH. Cutting Edge: NOX2 NADPH Oxidase Controls Infection by an Intracellular Bacterial Pathogen through Limiting the Type 1 IFN Response. J Immunol. 2021;206(2):323-8. https://doi.org/10.4049/jimmunol.2000694.

31. Ahmadi M, Bekeschus S, Weltmann KD, von Woedtke T, Wende K. Non-steroidal anti-inflammatory drugs: recent advances in the use of synthetic COX-2 inhibitors. RSC Med Chem. 2022;13(5):471-96. https://doi.org/10.1039/d1md00280e.

32. Mitsi E, Kamng'ona R, Rylance J, Solorzano C, Jesus Reine J, Mwandumba HC, et al. Human alveolar macrophages predominately express combined classical M1 and M2 surface markers in steady state. Respir Res. 2018;19(1):66. https://doi.org/10.1186/s12931-018-0777-0.

33. Hansakon A, Ngamphiw C, Tongsima S, Angkasekwinai P. Arginase 1 Expression by Macrophages Promotes Proliferation and Invasion into Brain Microvascular Endothelial Cells. J Immunol. 2023;210(4):408-19. https://doi.org/10.4049/jimmunol.2200592.

34. Sinclair C, Bommakanti G, Gardinassi L, Loebbermann J, Johnson MJ, Hakimpour P, et al. mTOR regulates metabolic adaptation of APCs in the lung and controls the outcome of allergic inflammation. Science. 2017;357(6355):1014-21. https://doi.org/10.1126/science.aaj2155.

35. Karcz TP, Whitehead GS, Nakano K, Nakano H, Grimm SA, Williams JG, et al. UDP-glucose and P2Y14 receptor amplify allergen-induced airway eosinophilia. J Clin Invest. 2021;131(7). https://doi.org/10.1172/JCI140709.

36. Petiz LL, Glaser T, Scharfstein J, Ratajczak MZ, Ulrich H. P2Y14 Receptor as a Target for Neutrophilia Attenuation in Severe COVID-19 Cases: From Hematopoietic Stem Cell Recruitment and Chemotaxis to Thrombo-inflammation. Stem Cell Rev Rep. 2021;17(1):241-52. https://doi.org/10.1007/s12015-021-10129-7.

37. Li HW, Jiang WJ, Ye SM, Zhou MZ, Liu CX, Yang XP, et al. P2Y14 receptor has a critical role in acute gouty arthritis by regulating pyroptosis of macrophages. Cell Death Dis. 2020;11(5). https://doi.org/10.1038/s41419-020-2609-7.

38. Liu L, Ito T, Li B, Tani H, Okuzaki D, Motooka D, et al. The UDP-glucose/P2Y14 receptor axis promotes eosinophil-dependent large intestinal inflammation. Int Immunol. 2024;36(4):155-66. https://doi.org/10.1093/intimm/dxad050.

39. Kvidera SK, Horst EA, Mayorga EJ, Sanz-Fernandez MV, Abuajamieh M, Baumgard LH. Estimating glucose requirements of an activated immune system in growing pigs. J Anim Sci. 2017;95(11):5020-9. https://doi.org/10.2527/jas2017.1830.

40. Li MZ, Li XW, Zhu L, Teng XK, Xiao HS, Shuai SR, et al. Differential expression analysis and regulatory network reconstruction for genes associated with muscle growth and adipose deposition in obese and lean pigs. Prog Nat Sci-Mater. 2008;18(4):387-99. https://doi.org/10.1016/j.pnsc.2007.10.011.

41. Gallina L, Cravotto C, Capaldi G, Grillo G, Cravotto G. Plant Extraction in Water: Towards Highly Efficient Industrial Applications. Processes. 2022;10(11). https://doi.org/10.3390/pr10112233.

42. Cho JY, Park SC, Kim TW, Kim KS, Song JC, Kim SK, et al. Radical scavenging and anti-inflammatory activity of extracts from Opuntia humifusa Raf. J Pharm Pharmacol. 2006;58(1):113-9. https://doi.org/10.1211/jpp.58.1.0014.

43. Minode M, Kadota K, Kawabata D, Yoshida M, Shirakawa Y. Enhancement in dissolution behavior and antioxidant capacity of quercetin with amino acids following radical formation via mechanochemical technique. Adv Powder Technol. 2022;33(5). https://doi.org/10.1016/j.apt.2022.103582.

44. Yang YF, Zhang LZ, Du XP, Zhang SF, Li LJ, Jiang ZD, et al. Recovery and purification of limonin from pummelo [Citrus grandis] peel using water extraction, ammonium sulfate precipitation and resin adsorption. J Chromatogr B Analyt Technol Biomed Life Sci. 2017;1060:150-7. https://doi.org/10.1016/j.jchromb.2017.05.036.

45. Phucharoenrak P, Muangnoi C, Trachootham D. A Green Extraction Method to Achieve the Highest Yield of Limonin and Hesperidin from Lime Peel Powder (Citrus aurantifolia). Molecules. 2022;27(3). https://doi.org/10.3390/molecules27030820.

46. Fan S, Zhang C, Luo T, Wang J, Tang Y, Chen Z, Yu L. Limonin: A Review of Its Pharmacology, Toxicity, and Pharmacokinetics. Molecules. 2019;24(20). https://doi.org/10.3390/molecules24203679.

Figure Legends

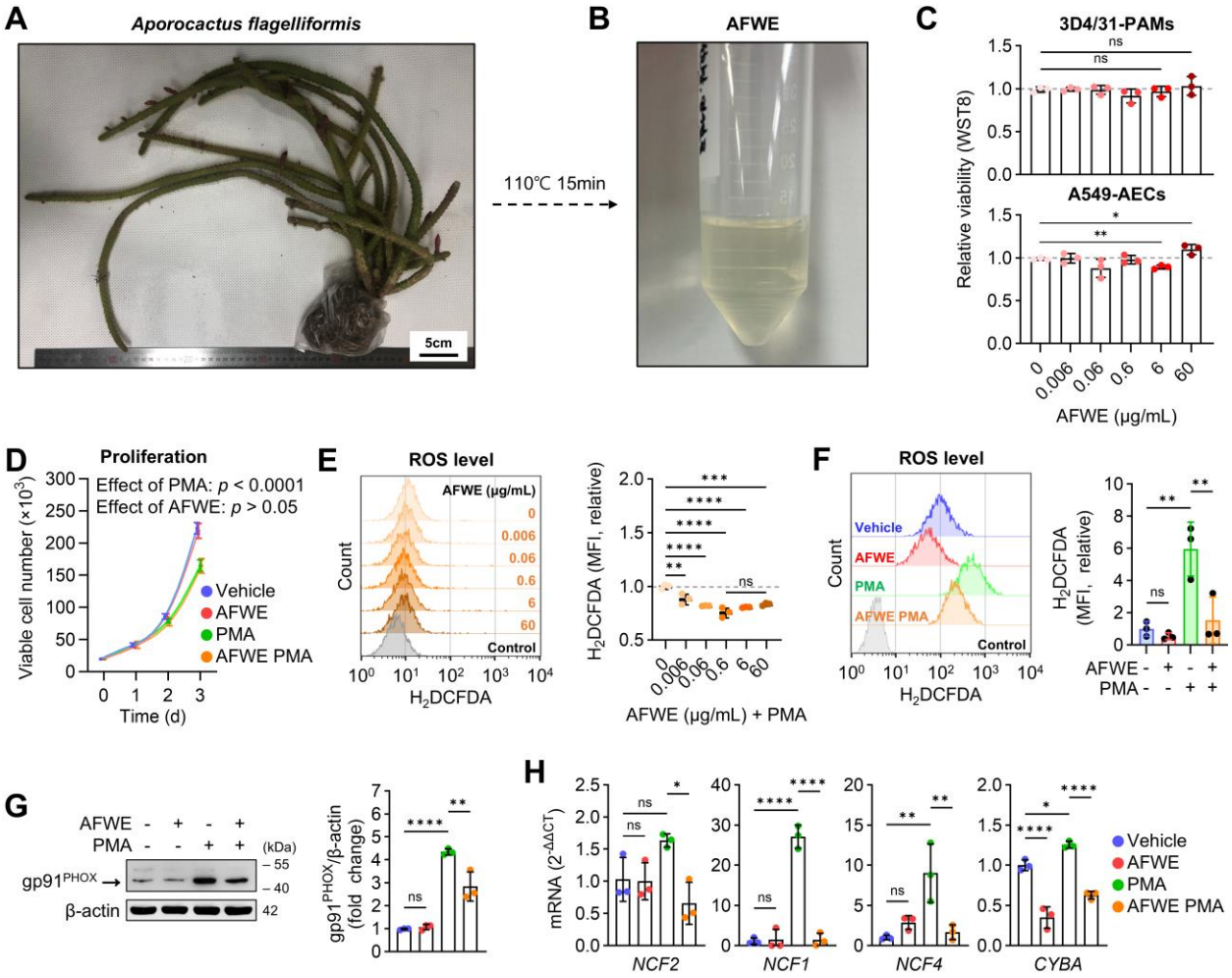

Fig. 1. Development of AFWE and its antioxidant effects on 3D4/31-PAMs. (A) Representative image of the *A. flagelliformis* used in this study. (B) Representative image of *A. flagelliformis* water extract (AFWE). (C) Viability of the 3D4/31-PAMs and A549-AECs treated with AFWE for 48 h (n = 3). *p* by two-tailed Student's T-test. (D) Proliferation of 3D4/31-PAMs treated with AFWE and PMA (n = 3). *p* by three-way ANOVA. (E-F) Intracellular ROS levels in 3D4/31-PAMs treated with AFWE for 24 h and PMA for 2 h (n = 3). (E) Dose-response screening of AFWE with PMA. (F) Intracellular ROS levels in the presence or absence of PMA. (G) Immunoblotting of $gp91^{PHOX}$ in 3D4/31-PAMs treated with AFWE for 24 h and PMA for 12 h (n = 3). (H) Expression of NOX-related genes in 3D4/31-PAMs treated with AFWE for 24 h and PMA for 4 h (n = 3). *p* by one-way ANOVA. $^{ns}p > 0.05$, $*p < 0.05$, $**p < 0.01$, $***p < 0.001$, and $****p < 0.0001$.

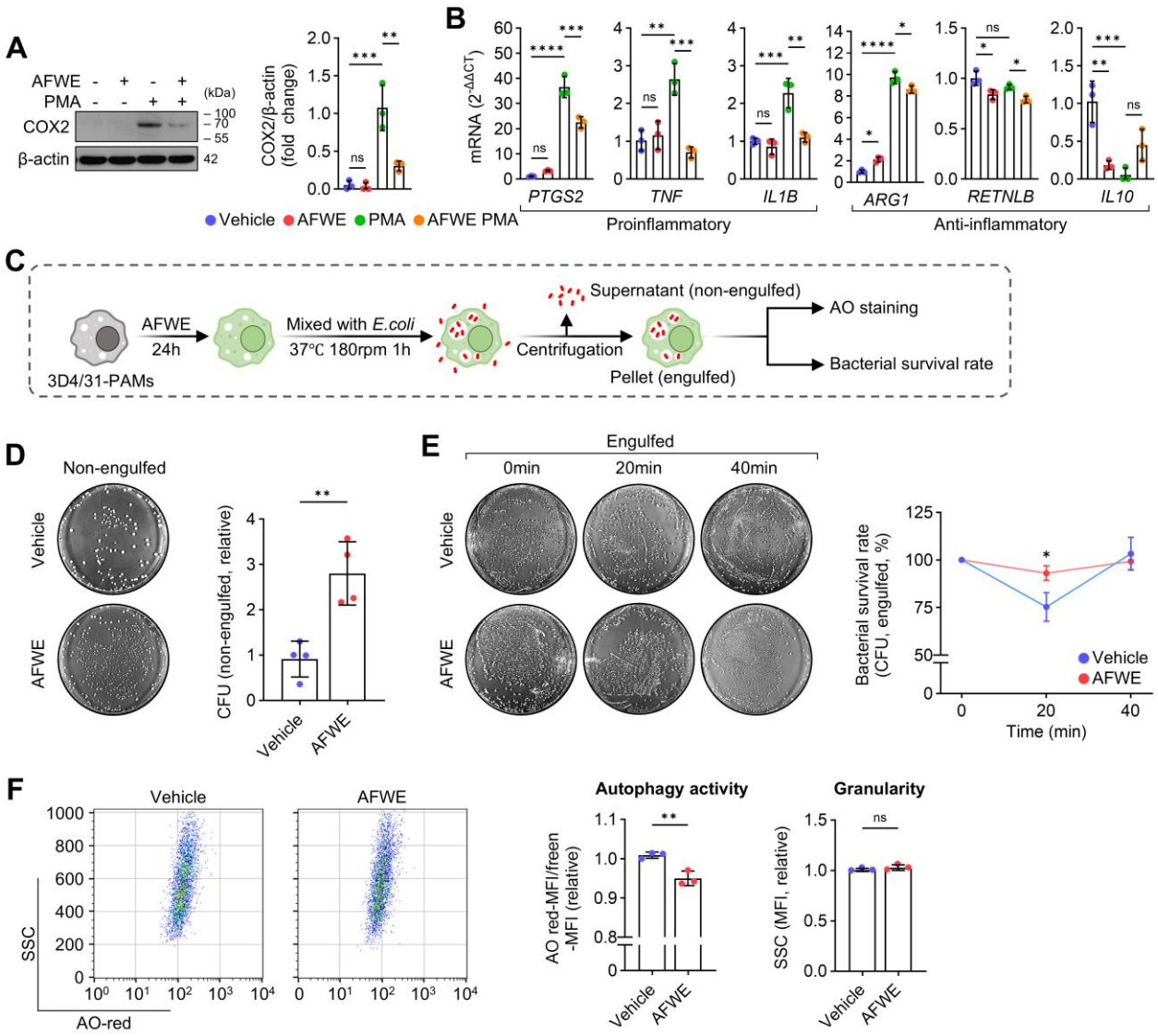

Fig. 2. AFWE suppresses proinflammatory gene expression and bactericidal activity in 3D4/31-PAMs. (A) Immunoblotting of COX2 in 3D4/31-PAMs treated with AFWE for 24 h and PMA for 12 h. (B) Expression of inflammation-related genes in 3D4/31-PAMs treated with AFWE for 24 h and PMA for 4 h. *p* by one-way ANOVA. (C-F) *In vitro* bactericidal assay of 3D4/31-PAMs treated with AFWE for 24 h. (C) Graphical scheme of *the in vitro* bactericidal assay. (D) Representative images and levels of non-engulfed bacteria (n = 4). *p* by unpaired two-tailed Student's t-test. (E) Representative images and bacterial survival rates (normalized to each time point at 0 h) (n = 3). *p* by two-way ANOVA. (F) Autophagic activity was quantified using flow cytometry with acridine orange (AO). Intracellular granularity (SSC, side scatter) is shown (n = 3). *p* by unpaired two-tailed Student's t-test. $^{ns}p > 0.05$, $*p < 0.05$, $**p < 0.01$, $***p < 0.001$, and $****p < 0.0001$.

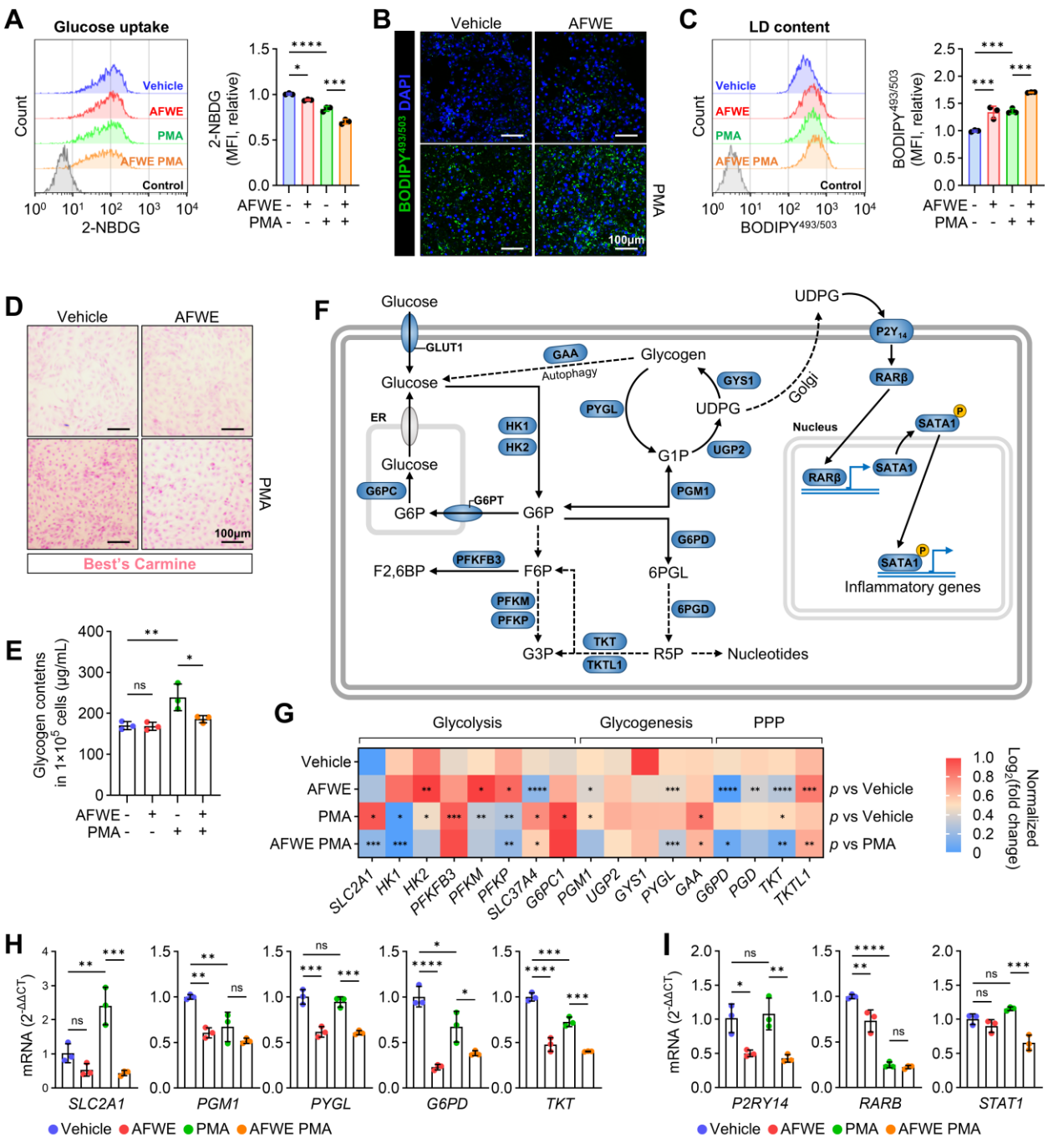

Fig. 3. AFWE suppresses P2Y$_{14}$- associated metabolism in 3D4/31-PAMs. (A) The glucose uptake rate in 3D4/31-PAMs treated with AFWE for 24 h and PMA for 2 h (n = 3). (B-D) 3D4/31-PAMs treated with AFWE for 24 h and PMA for 24 h (n = 3). (B-C) Fluorescence microscopy (B) and flow cytometry (C) of LD content in 3D4/31-PAMs. (D) Best's Carmine glycogen staining. (E) Quantification of glycogen content by using anthrone. (G-I) Expression of genes related to P2Y$_{14}$ activation in 3D4/31-PAMs treated with AFWE for 24 h and PMA for 4 h (n = 3). (G) Normalized Log$_2$(fold change) of the genes. (H-I) Representative gene expression. *p* by one-way ANOVA. $^{ns}p > 0.05$, $^{*}p < 0.05$, $^{**}p < 0.01$, $^{***}p < 0.001$, and $^{****}p < 0.0001$.

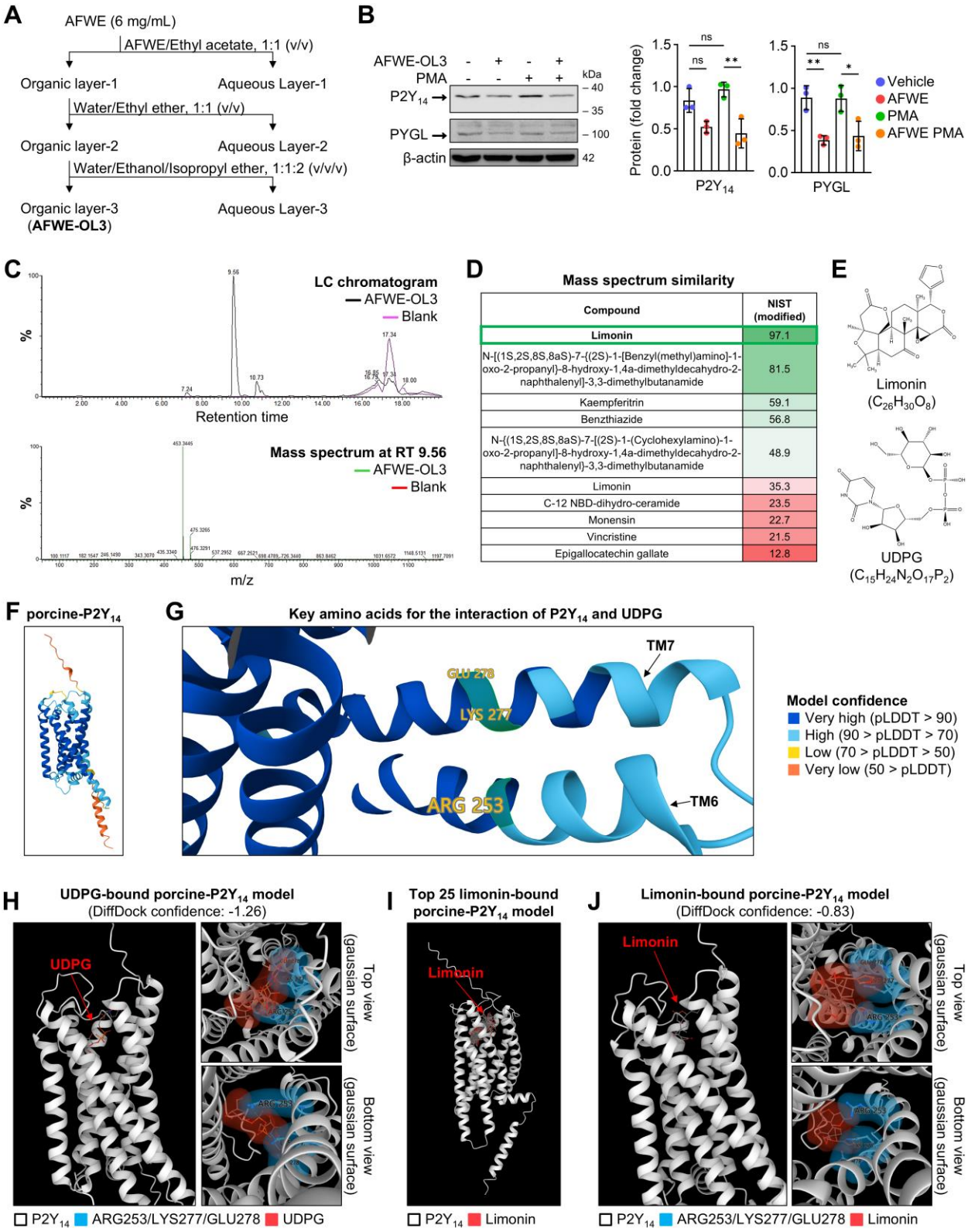

Fig. 4. Identification of anti-inflammatory substances in AFWE. (A) Experimental scheme for fractionation of AFWE. (B) Immunoblotting of $P2Y_{14}$ and PYGL in 3D4/31-PAMs treated with 73 μg/mL AFWE-OL3 for 24 h and

with PMA for 12 h (n = 3). *p* by one-way ANOVA. $^{ns}p > 0.05$, $*p < 0.05$, and $**p < 0.01$. (C) LC-MS spectrum of the AFWE-OL3. (D) Mass spectrum similarity based on modified NIST (National Institute of Standards and Technology) score. (E) Structure of limonin and UDPG. (F-G) Protein structural model of porcine-$P2Y_{14}$ (F) and the positions of ARG253, LYS277, and GLU278 (G) in porcine-$P2Y_{14}$ (TM, transmembrane). Colored by model confidence (pLDDT, per-residue confidence score). (H) Predicted model for the UDPG-bound porcine-$P2Y_{14}$. (I-J) Prediction model for limonin-bound porcine-$P2Y_{14}$. (I) Top 25 modes. (J) Representative model with the highest DiffDock confidence level.

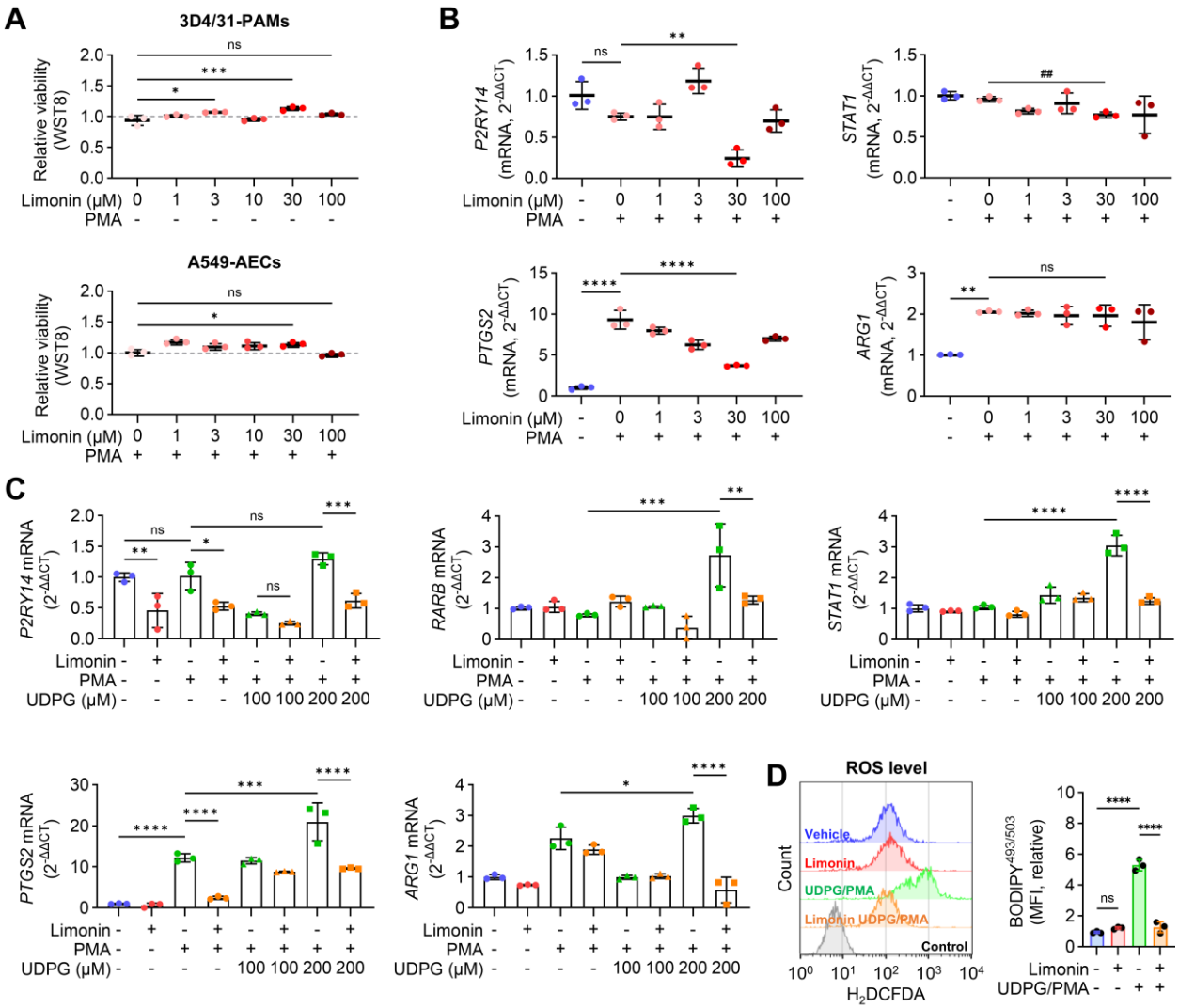

Fig. 5. Limonin suppresses $P2Y_{14}$-associated proinflammatory features in 3D4/31-PAMs. (A) Viability of 3D4/31-PAMs and A549-AECs treated with limonin for 24 h and PMA for 24 h (n = 3). (B) Inflammatory gene expression in 3D4/31-PAMs treated with limonin for 24 h and PMA for 4 h (n = 3). $^{\#\#}p < 0.01$ by unpaired two-tailed Student's t-test. (C) Expression of genes related to $P2Y_{14}$ activation in 3D4/31-PAMs treated with limonin for 24 h and PMA/UDPG for 4 h. (D) Intracellular ROS levels in 3D4/31-PAMs treated with AFWE for 24 h and PMA/UDPG for 2 h (n = 3). *p* by one-way ANOVA. *p* by one-way ANOVA, $^{ns}p > 0.05$, $^{*}p < 0.05$, $^{**}p < 0.01$, $^{***}p < 0.001$, and $^{****}p < 0.0001$.

525 # Tables and Figures

526 **Table 1. Antibodies used in this study for immunoblotting**

Antibody (dilution)	Catalog No.	Manufacturers
Anti-β-actin antibody (1:10000)	A5441	Sigma-Aldrich
Anti-gp91^{PHOX} antibody (1:1000)	sc-20782	Santa Cruz Biotechnology
Anti-COX2 antibody (1:500)	sc-19999	Santa Cruz Biotechnology
Anti-P2Y$_{14}$ antibody (1:500)	ab136264	Abcam
Anti-PYGL antibody (1:500)	ab190243	Abcam
Anti-mouse IgG, HRP-linked antibody (1:5000)	#7076	Cell signaling
Anti-rabbit IgG, HRP-linked antibody (1:5000)	#7074S	Cell signaling

527

528 **Table 2. Primers sequences used in this study for qRT-PCR**

Gene symbol (accession)	Sense (5' to 3')	Antisense (5' to 3')
RPS29 (NM_001001633.2)	CGGAAATACGGCCTCAATATG	GCCAATATCCTTCGCGTACTG
NCF2 (NM_001123142.1)	GTGAATGAAGAGTGGCCGGA	CAAATCTGTGGTTGCGCGTT
NCF1 (NM_001113220.1)	GCGGGGAATCCATTGCAAAA	CTGCAACGGTGCAAGATGAG
NCF4 (XM_013997542.2)	GTGCAGCTCATGGTGAGACA	TGGGTGATATGCAGCTTCCAG
CYBA (NM_214267.1)	GGAGCGCTGCGAACAAAAGT	CAGGAAGGCCCGGATGTAGT
PTGS2 (NM_214321.1)	AATGGACGATGAACGGCTG	TGAAGTGGTAGCCACTCAGG
TNF (NM_214022.1)	CGTTGTAGCCAATGTCA	TAGGAGACGGCGATGC
IL1B (NM_214055.1)	TGCAAGGAGATGATAGCAACAAC	TCTCCATGTCCCTCTTTGGGT
ARG1 (NM_214048.2)	GTGGACCCTGCAGAACACTA	ACCTTGCCAATTCCCAGCTT
RETLNB (NM_001103210.1)	AATCGCAAGGGGTTCTCAGT	TTGGAGCAGAGGGATTGAGC
IL10 (NM_214041.1)	CGGCGCTGTCATCAATTTCT	GGCTTTGTAGACACCCCTCTC
SLC2A1 (XM_021096908.1)	CTGCTCATCAACCGCAATGA	GGCTCTCCTCCTTCATCTCC
HK1 (NM_001243184.1)	GCACGATGTGGTGACCTTAC	CCAGTCCCTACGATGAGTCC
HK2 (NM_001122987.1)	CACTGCTGAAGGAAGCCATC	GGGTCTTCATAGCCACAGGT
PFKFB3 (XM_021065026.1)	GGACCGATGTTACCTTTGCC	TTGGCGTGGTTCAGTCTTTC
PFKM (DQ363336.1)	CGCTCCACTGTGAGAATTGG	GCTAAGCCCTCAAAGCCATC
PFKP (XM_021065066.1)	CCGACGGACACAAGATGTTC	TTGTCCCAAGAATGGAGCCT
SLC37A4 (NM_001199719.1)	CTGTGGTCAGAAGCTCGTGT	GGAGAAGGTCTTGCGGTTGA
G6PC1 (NM_001113445.1)	TTACCTGCTGCTAAAGGGGC	ACATGCTGGAGTTGAGAGCC
PGM1 (NM_001246318.1)	CCTGTGGACGGAAGCATTTC	ATGTACAGTCGGATGGTGGC
UGP2 (NM_213980.1)	GCAGTAGGGGCTGCCATTAAA	GCACGGTAGGAAATTCTCGC
GYS1 (AJ507152.1)	TAGGCCGGGTATAACTCCCT	AAAGGGGCCGCAACCATTA
PYGL (NM_001123172.1)	CACCTGCATTTCACACTGGTC	AGTAGTACTGCTGCGTGCG
GAA (XM_021066505.1)	CCTACACGCAGGTCGTCTTC	GTTGGAGACAGGAACACCGT
G6PD (XM_021080744.1)	GCGAGAAACTCCAGCCCATT	GTAGGTGCCCTCGTACTGGA
PGD (XM_003127557.4)	TACTTCGGGGCTCACACCTA	GTACGAAGAGGAGGACACGC
TKT (NM_001112681.1)	GGGACAAGATAGCTACCCGC	TAGCACTCGATGAAGCGGTC
TKTL1 (XM_021080741.1)	CTACCCAGAAGGTGGCATCG	GATGGACCAGGATGTCAGGC
P2RY14 (XM_021069620.1)	CCACATTGCCAGAATCCCCT	CAGGCATACATTTGCAGCCG
RARB (XM_005669304.3)	CTCCGCAGCATCAGTGCTAA	TGGGGTCAAGGGTTCATGTC
STAT1 (NM_213769.1)	CAAAGGAAGCCCCAGAACCT	CCCACCATTCGAGACACCTC

529

530 **Figure 1_Revised.**

531

532 **Figure 2.**

533

534 **Figure 3.**

535

536 **Figure 4.**

537

538 **Figure 5_Revised.**